CHAPTER 8

Advanced Methods for SPR Imaging Biosensing

ALASTAIR W. WARK, HYE JIN LEE AND ROBERT M. CORN

Department of Chemistry, University of California–Irvine, Irvine, CA 92697, USA

8.1 Introduction

Microarray biosensors have become an invaluable biotechnological tool for the rapid, multiplexed detection of surface bioaffinity interactions. For example, nucleic acid microarrays are currently being applied to the areas of genomics [1,2], genetic testing [3], gene expression [4,5], and single nucleotide polymorphism (SNP) genotyping [6,7]. Many researchers are also interested in developing protein microarrays for application in the areas of proteomics [8–10] and drug discovery [11,12]. In addition, the detection and profiling of multiple protein biomarkers in biological fluids (*e.g.* blood, serum, urine) by antibody microarrays is a potentially powerful method for the diagnosis of diseases and the monitoring of subsequent therapeutic treatments [13,14].

An attractive alternative to traditional fluorescence-based microarray detection methods is the surface-sensitive optical technique of surface plasmon resonance imaging (SPRI). SPRI, also denoted SPR microscopy [15–17], was originally applied to the study of surface morphology in phospholipid monolayers and other thin surface films [15]. Since those initial efforts, SPRI has evolved into a primary method for the measurement of bioaffinity adsorption onto biopolymer microarrays by detecting changes in the local refraction index upon binding [18–31]. This is a significant advantage in the analysis of biological samples where labeling multiple biomarkers with fluorophores or nanoparticles is often not possible. Over the last decade, a number of improvements have been made in SPRI in terms of instrumentation, surface microarray fabrication and microfluidic formats for the multiplexed measurement of

surface adsorption kinetics with microarrays. A brief review of some of these advances is given in Section 8.2.

While multiplexed microarray analysis of bioaffinity interactions is a valuable research tool, even more specificity and sensitivity can be obtained by coupling the bioaffinity process to an enzymatic transformation. This coupling is often employed in solution-phase biotechnological processes; for example, coupling of DNA hybridization with polymerase chain reaction (PCR) leads to the process of PCR amplification in genomic DNA samples [32,33]. However, the direct incorporation of solution enzymatic methods such as PCR into a parallel microarray format is difficult, because any intermediate solution species will diffuse on to neighboring array elements. Instead of using solution enzyme chemistry, it is better to utilize a surface enzyme reaction on biomolecules attached to the microarray surface. The use of surface enzyme chemistry ensures that the parallel nature of the multiplexed microarray assay remains intact. In Section 8.3, we describe some of the basic equations that we have developed for the use of surface enzyme kinetics in SPRI, and a new enzymatically amplified SPRI methodology to detect DNA down to femtomolar concentrations.

Finally, in Section 8.4 we describe how the incorporation of DNA-coated gold nanoparticles into the enzymatically amplified SPRI methodologies can further increase the sensitivity of these array bioaffinity measurements. DNA-coated gold nanoparticles were originally employed with SPRI by He *et al*. to detect DNA in a sandwich assay format at a concentration of 10 pM [30]. Using a nanoparticle-enhanced surface ligation strategy, we demonstrate SNP genotyping with SPRI down to a concentration of 1 pM, and with a combination of poly(A) polymerase and DNA-coated gold nanoparticles, we can detect microRNA in biological samples down to a concentration of 10 fM [34].

8.2 Advances in SPRI Instrumentation and Surface Chemistry

Since the first demonstration in 1997 of the use of SPRI and microarrays for monitoring DNA–DNA interactions [35,36], our group has continued to develop this technology focusing in particular on (i) optimizing the SPRI instrumental set-up and (ii) designing new chemical strategies for the surface attachment of different biomolecular probes in an array format. A schematic diagram of an SPRI apparatus is shown in the middle inset in Figure 8.1, where the output from a collimated white light source is passed through a polarizer and then directed on to the prism/chip assembly at a fixed optimal angle. The reflected p-polarized light is then collected via a narrow-band interference filter centered at 830 nm on to a CCD camera. We have found that this white light–NIR filter combination has several advantages compared with the use of a visible monochromatic laser beam such as improved sensitivity and the removal of interference fringes from the SPR image that are often problematic when using coherent laser excitation [37]. A number of commercial SPR imaging

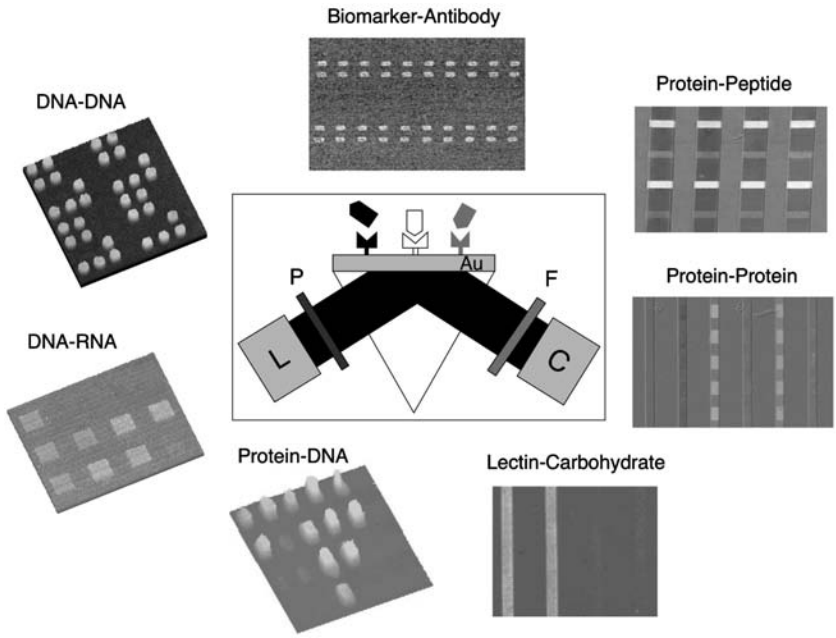

Figure 8.1 A simplified SPRI set-up (middle inset) and representative SPRI difference images obtained for the detection of bioaffinity interactions with biopolymer microarrays. From top center and clockwise, protein biomarker binding to an antibody microarray, antibody binding to a peptide microarray, protein interactions with a His-tagged protein microarray, lectin binding to a carbohydrate line array, response regulator protein binding to a dsDNA microarray, 16mer ssDNA hybridization adsorption on an ssRNA microarray and 16mer ssDNA hybridization adsorption on an ssDNA microarray. The middle inset shows a simplified SPRI set-up. Briefly, the output from a collimated white light source (L) is passed through a polarizer (P) with the resulting p-polarized light directed on to a high index prism–sample assembly at an optimal incident angle. The reflected light from the sample assembly is then collected via a narrow band pass filter (F) on to a CCD camera (C).

instruments are now available from GWC Technologies, Biacore (HTS Biosystems), IBIS Technologies and GenOptics; for more on instrumental aspects, see Chapter 3.

In conjunction with SPRI instrumentation, the use of well-characterized and robust surface chemistries to tether biological molecules to gold surfaces in an array format is extremely important for successful SPRI biosensing measurements. Consequently, we have developed a variety of surface immobilization strategies for covalently attaching different biomolecular probes to chemically modified gold surfaces [38–41]. These attachment chemistries can be used along with either UV photopatterning [39] or microfluidic techniques [42] to create arrays of multiple, independently addressable elements on a single surface.

Figure 8.1 shows a set of representative SPRI images obtained from various studies that our group has performed [18,34,43–52]. A detailed summary of the biopolymer microarrays (*e.g.* DNA, RNA, peptide, protein, carbohydrate) prepared for different biomolecular targets is listed in Table 8.1.

A third area in which SPRI biosensing has improved is in examining the thermodynamic and kinetic parameters of surface bioaffinity interactions. A simple one-step surface bioaffinity adsorption process involving the specific binding of a target biomolecule (T) to a surface attached probe (P) or ligand

Table 8.1 Summary of different surface bioaffinity measurements performed using SPRI and biopolymer microarrays.

Microarray probes (on surface)	*Target biomolecules (in solution)*	K_{ads} (M^{-1})	*Ref.*
DNA	**DNA**		
ssDNA	ssDNA (16–18 bases)	2.0×10^7	45,53
DNA	**RNA**		
ssDNA	ssRNA (18 bases)	1.8×10^7	53
SsDNA	16S ribosomal RNA	*N*	86
	Messenger RNA		42
DNA	**Proteins**		
Biotinylated DNA	Streptavidin	*N*	35
ssDNA	ssDNA binding protein	*N*	87
dsDNA	Mismatch binding proteins	*N*	87
dsDNA	Phosphorylated OmpR	1.6×10^8	50
dsDNA	Phosphorylated VanR	6.6×10^6	50
Peptides	**Antibodies and proteins**		
Flag-peptide	Anti-Flag	1.5×10^8	51
S-peptide	S-protein	1.7×10^7	52
Carbohydrates	**Lectins**		
Mannose	Concanavalin A	2.2×10^7	88
Galactose	Jacalin	5.6×10^6	88
Proteins	**Antibodies and DNA**		
His-tagged ubiquitin	Anti-ubiquitin	*N*	89
His-tagged Flag	Anti-Flag	*N*	89
His-tagged RFP	Anti-RFP	*N*	89
His-TATA box-binding protein	dsDNA	*N*	89
Antibodies	**Protein biomarkers**		
Anti-β_2-microglobulin	β_2-Microglobulin	1.4×10^8	43
Anti-cystatin C	Cystatin C	1.0×10^8	43
RNA	**Proteins**		
RNA aptamer	factor IXa	1.6×10^7	71

RFP, red fluorescent protein; ssDNA, single-stranded DNA; dsDNA, double-stranded DNA; *N*, not measured with SPRI.

can be described by the reaction

$$\mathrm{T} + \mathrm{P} \underset{k_\mathrm{d}}{\overset{k_\mathrm{a}}{\rightleftharpoons}} \mathrm{TP} \tag{8.1}$$

where TP is the surface-bound target–probe complex and the rates of T adsorption and desorption are defined by k_a and k_d, respectively (see Figure 8.2a). An example of such a reaction would be DNA hybridization adsorption on a DNA microarray. Figure 8.2b shows an SPRI difference image of a four-component ssDNA microarray following exposure to two complementary 16mer DNA target sequences. A positive increase in percentage reflectivity ($\Delta\%R$) is observed at only the perfectly matched array elements due to the formation of duplexes via hybridization adsorption. Fresnel calculations and experimental evidence show that if the SPRI response remains below 10%, then it is directly proportional to the relative surface coverage (θ) of complementary DNA [53], where $\theta = \Gamma_{\mathrm{TP}}/\Gamma_{\mathrm{tot}}$ and Γ represents the molecular surface density. At equilibrium, the fractional surface coverage reaches a steady state and this

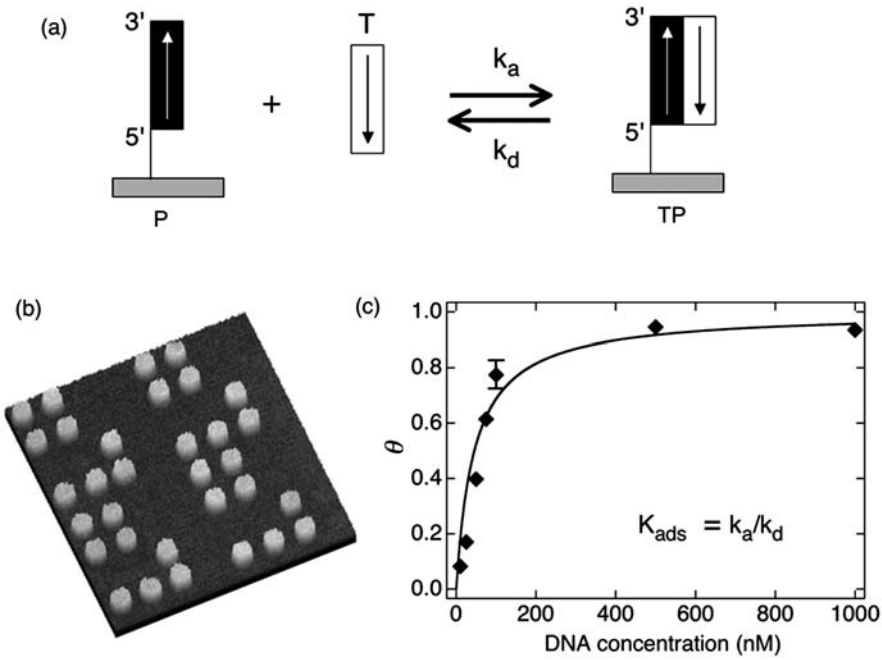

Figure 8.2 (a) Schematic showing target ssDNA (T) hybridization adsorption on ssDNA microarray elements (P). (b) SPRI difference image obtained for sequence-specific 16mer target ssDNA hybridization adsorption on ssDNA microarray elements. (c) A representative plot of relative surface coverage (θ) as a function of target DNA concentration. The solid line is a Langmuir isotherm fit to the data, from which a value of $K_{\mathrm{ads}} = 2 \times 10^7\,\mathrm{M}^{-1}$ was determined.

equilibrium surface coverage θ_{eq} is given by the Langmuir adsorption isotherm:

$$\theta_{eq} = \frac{K_{ads}[T]}{1 + K_{ads}[T]} \tag{8.2}$$

where the Langmuir adsorption coefficient K_{ads} is defined as $K_{ads} = k_a/k_d$. Figure 8.2c shows a typical Langmuir isotherm plot of θ versus concentration for 16mer DNA from which a value of $K_{ads} = 2\times10^7\,M^{-1}$ was obtained [45,53]. At low surface coverages, the Langmuir isotherm depends linearly on DNA concentration and eq. (8.2) becomes $\theta_{eq} = K_{ads}[T]$. In DNA hybridization adsorption, the lowest DNA concentration observed with SPRI was 1 nM, which corresponds to a θ_{eq} of 0.02.

In addition to equilibrium measurements, further information on surface bioaffinity interactions can be obtained by measuring the kinetic parameters k_a and k_d. For the case of adsorption from a solution of concentration [T] on an unoccupied surface, the time-dependent fractional surface coverage, $\theta(t)$, is given by

$$\theta(t) = \theta_{eq}[1 - e^{-(k_a[T]+k_d)t}] \tag{8.3}$$

where θ_{eq} is the equilibrium value for θ at a particular bulk concentration, as given using eq. (8.2). For the case when $\theta = 1$ at $t = 0$, the desorption rate can be described by

$$\theta(t) = \theta_{eq}e^{-(k_d)t} \tag{8.4}$$

Equations (8.3) and (8.4) have been used frequently to analyze the adsorption of biomolecules on surfaces, especially with SPR [54] and SPRI [52]. Compared with single-channel SPR measurements, real-time SPRI has a great advantage in being able to determine simultaneously the rates of target adsorption/adsorption at multiple different probe elements on a single chip.

Figure 8.3a shows the design of a PDMS microchannel flow cell that facilitates well-controlled and reproducible sample delivery to each array element in addition to significantly reducing the sample volume ($\sim$10 µl). SPR imaging kinetic experiments are performed using a continuous flow-through microchannel to prevent mass transport limitations, whereas equilibrium measurements are obtained under stopped-flow conditions using a larger volume flow cell ($\sim$100 µl). Additionally, a specially designed water-jacketed flow cell, which controls the system temperature to within 0.1 °C, is used to perform temperature-dependent studies. We have applied real-time SPRI to determine accurately the k_a and k_d of S protein binding to an array composed of various S peptide analogues [52]. For this study, custom-written software that rapidly acquires and organizes large data sets during real-time acquisition was used (see Figure 8.3b). These real-time SPRI methods have also been employed to characterize quantitatively our surface enzyme methods described in Section 8.3.

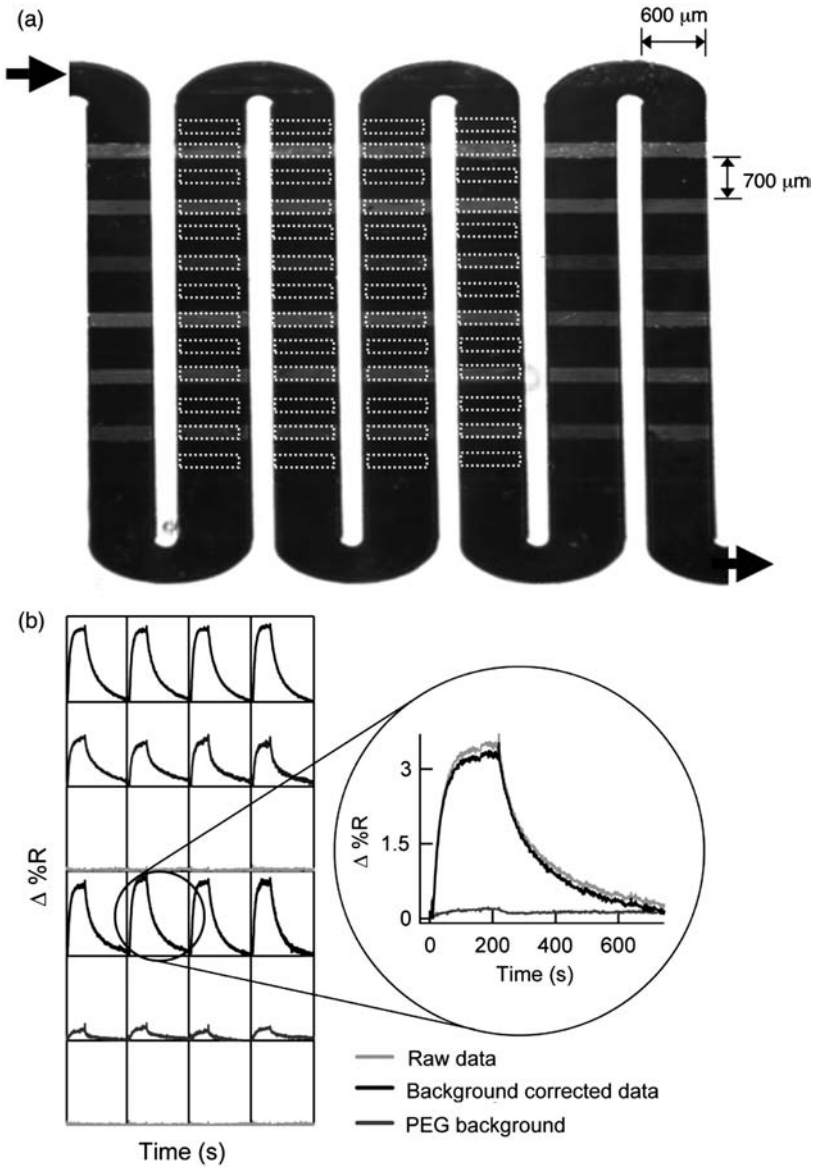

Figure 8.3 (a) SPRI raw image of a peptide array created from parallel PDMS microfluidic channels to deliver heterobifunctional cross-linker and probe molecules before being replaced by a second serpentine PDMS channel to create a continuous flow cell for use in kinetics measurements. The dotted lines indicate regions of interest (ROIs) on the array where the change in percent reflectivity is measured as a function of time. (b) Simultaneous real-time SPRI measurements obtained for each ROI [peptide elements and poly(ethylene glycol) background] when the array was first exposed to a 150 nM solution of S protein and then rinsed with phosphate buffer only. The SPRI signal increases then decreases in response to protein adsorption/desorption. The adjacent poly(ethylene glycol) regions are used to correct the SPRI signal for background effects. Reprinted with permission from reference 52.

Finally, we have also continued to pursue the development of improved SPRI biosensing methods; one example is the design of novel multiple-layered chip structures that support the generation of long-range plasmons (LRSPs) [45,55–58]. Essential to the LRSPR chip design shown in Figure 8.4 is the use of Cytop as an inert optically transparent material whose refractive index is very close to that of water, with the depth and position of the LRSPR mode strongly dependent on the thickness of both the Cytop and gold films. Compared with conventional surface plasmons, LRSPs possess longer surface propagation lengths, higher electric field strengths and narrower resonance curves. This is demonstrated in Figure 8.4a, which shows *in situ* scanning angle reflectivity measurements obtained for both a conventional SPRI chip design [SF10] and that of a LRSPR chip [SF10 prism/Cytop (1180 nm)/gold (32 nm)/water [45].

To demonstrate the advantages of LRSPR, DNA microarrays were prepared on both conventional and long-range chips. Repeated measurements of DNA hybridization adsorption showed an $\sim 20\%$ increase for the LRSPR $\Delta\%R$ signal compared with regular SPRI chips. Perhaps of more interest is the much higher surface electric field strengths associated with the generation of LRSPs. Figure 8.4b displays the results of n-phase Fresnel calculations [59,60] which demonstrate that the LRSP electric field intensity at the gold sensing surface is higher by as much as 10^3 compared with that associated with conventional surface plasmons. These enhanced fields should lead to further research advances in surface plasmon fluorescence spectroscopy (SPFS) studies [61].

8.3 Surface Enzymatic Transformations for Enhanced SPRI Biosensing

To enhance further the biosensing capabilities of SPRI and overcome some of the difficulties associated with detecting very low target concentrations (< 1 nM), we have developed a number of advanced methodologies which couple surface enzyme reactions and bioaffinity interactions on biopolymer microarrays [18,34,46,48,49]. In this section, we first outline a simple theoretical framework that quantitatively describes the catalysis reaction of an enzyme in bulk solution with a surface immobilized substrate. The application of this model to analyze real-time SPRI and SPFS measurements of RNase H surface activity is also discussed. Next, we provide two examples of surface enzymatic processes on nucleic acid microarrays that are coupled with surface bioaffinity interactions to enhance the sensitivity and selectivity of the biosensor. These processes are (i) the enzymatic amplified detection of genomic DNA using RNase H and RNA microarrays and (ii) the application of surface ligation chemistry for the fabrication of RNA microarrays from DNA microarray templates for the study of protein–RNA aptamer interactions.

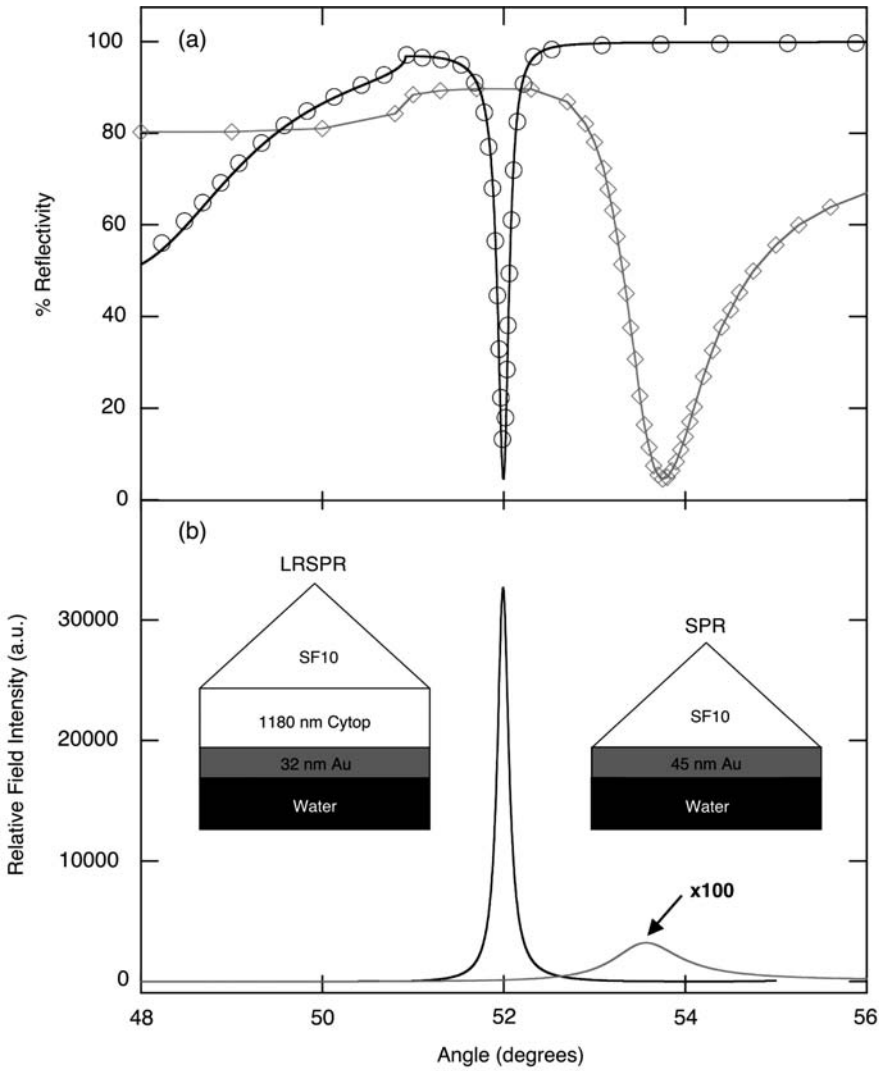

Figure 8.4 (a) SPR reflectivity curves of p-polarized light as a function of incident angle for a long-range SF10 glass/Cytop (1180 nm)/Au (32 nm)/water configuration (○) and a conventional SF10 glass/Au (45 nm)/water SPRI configuration (◇) at excitation wavelength 814 nm. The solid lines show the results of a theoretical fit to the data using a multiple phase Fresnel calculation. Refractive indices (n) used in the calculation: $n(\mathrm{SF10}) = 1.711$, $n(\mathrm{Cytop}) = 1.336$, $n(\mathrm{Cr}) = 3.186 + 3.47\mathrm{i}$, $n(\mathrm{Au}) = 0.185 + 5.11\mathrm{i}$ and $n(\mathrm{H_2O}) = 1.328$. (b) Calculated relative optical field intensities for the LRSPR and conventional SPR assemblies whose schematics are shown as insets. The conventional SPR field intensity is multiplied by 100 for visibility. Reprinted with permission from reference 45.

8.3.1 Measuring Surface Enzyme Kinetics

The quantitative characterization of the surface enzyme reactions utilized in advanced SPRI biosensing methods is extremely important, as an enzyme can react orders of magnitude slower on a surface as compared with in solution. Here, we describe a simple kinetic model that includes enzyme adsorption, desorption and the surface enzymatic reaction and apply it to the analysis of real-time SPRI and SPFS measurements of the surface hydrolysis of RNA–DNA heteroduplexes[1] by RNase H. This surface reaction (see Figure 8.5, inset) forms the basis of our enzymatic amplification methodology described in Section 8.3.2. For the case of a 1:1 binding of an enzyme molecule (E) to a surface-immobilized substrate (S), we have identified three processes that control the overall reaction rate:

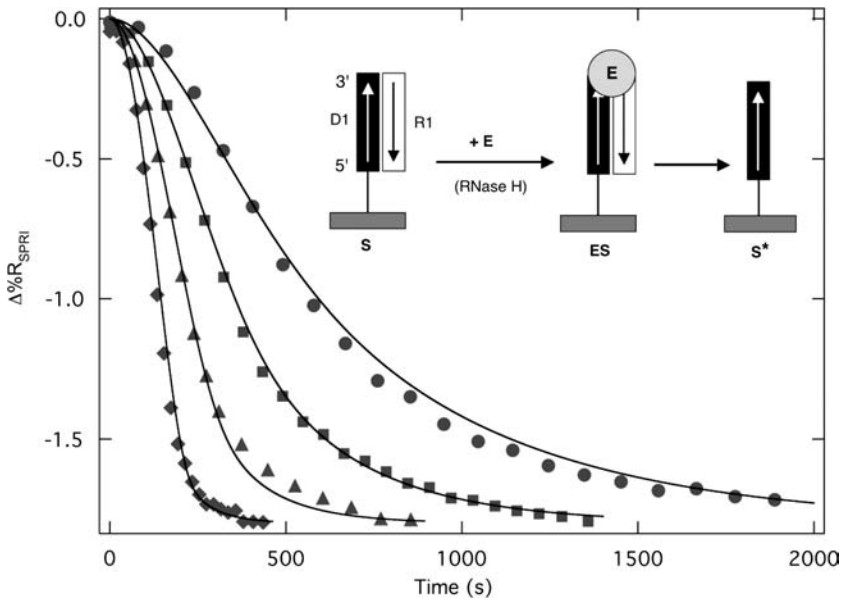

Figure 8.5 A series of real-time SPRI data curves obtained for the RNase H hydrolysis of surface RNA–DNA (R1-D1) array elements at different concentrations of RNase H solutions [0.5 nM (?), 1.0 nM (?), 2.0 nM (▲) and 4.0 nM (?)]. The experimental curves were globally fitted using eqs. (8.8)–(8.10) to obtain the parameter values $k_a = 3.4\ (\pm 0.2) \times 10^6\,M^{-1} \cdot s^{-1}$, $k_d = 0.10\ (\pm 0.05)\,s^{-1}$, $k_{cat} = 1.0\ (\pm 0.1)\,s^{-1}$ and $\beta = 180\ (\pm 20)$. The solid lines are the fitted theoretical kinetic curves. The inset is a schematic illustration of the RNase H hydrolysis of surface RNA–DNA heteroduplexes. Reprinted with permission from reference 64.

AQ3

[1] A heteroduplex is a double-stranded molecule of nucleic acid composed of two single complementary strands derived from different sources.

$$\mathrm{E}_{(x=\infty)} \xrightarrow{k_\mathrm{m}} \mathrm{E}_{(x=0)} \tag{8.5}$$

$$\mathrm{S} + \mathrm{E}_{(x=0)} \underset{k_\mathrm{d}}{\overset{k_\mathrm{a}}{\rightleftharpoons}} \mathrm{ES} \tag{8.6}$$

$$\mathrm{ES} \xrightarrow{k_\mathrm{cat}} \mathrm{S}^* + \mathrm{E}_{(x=0)} \tag{8.7}$$

where $\mathrm{E}_{(x=\infty)}$ and $\mathrm{E}_{(x=0)}$ are the bulk and surface enzyme concentrations, respectively, ES is the surface enzyme–substrate complex, S* is the surface-bound product and k_cat is the surface reaction rate for the enzyme complex. When microfluidics are used for solution delivery, the enzyme diffusion can be described by a steady-state mass transport coefficient (k_m) that can also be written as D/δ, where D is the diffusion coefficient for the enzyme and δ is the steady-state diffusion layer thickness [62,63].

The kinetic equations for this reaction scheme can be expressed in terms of the relative fractional surface coverages of each of the three surface species (denoted $\theta_x = \Gamma_x/\Gamma_\mathrm{tot}$, where $x = S$, ES or S^*):

$$\theta_\mathrm{S} + \theta_\mathrm{ES} + \theta_{\mathrm{S}^*} = 1 \tag{8.8}$$

$$\frac{\mathrm{d}\theta_\mathrm{ES}}{\mathrm{d}t} = \frac{k_\mathrm{a}[E](1 - \theta_\mathrm{ES} - \theta_{\mathrm{S}^*}) - (k_\mathrm{d} + k_\mathrm{cat})\theta_\mathrm{ES}}{1 + \beta(1 - \theta_\mathrm{ES} - \theta_{\mathrm{S}^*})} \tag{8.9}$$

$$\frac{\mathrm{d}\theta_{\mathrm{S}^*}}{\mathrm{d}t} = k_\mathrm{cat}\theta_\mathrm{ES} \tag{8.10}$$

In eq. (8.9), [E] is the bulk enzyme concentration and β is the dimensionless diffusion parameter [62,63], defined by

$$\beta = \frac{k_\mathrm{a}\Gamma_\mathrm{tot}}{k_\mathrm{m}} = \frac{k_\mathrm{a}\Gamma_\mathrm{tot}\delta}{D} \tag{8.11}$$

These equations were derived in a series of recent papers [18,64,65] and can be solved using simple Euler integration methods with the initial conditions $\theta_\mathrm{S} = 1$ and $\theta_\mathrm{ES} = \theta_{\mathrm{S}*} = 0$ at time $t = 0$ to yield three time-dependent surface coverages $\theta_\mathrm{ES}(t)$, $\theta_{\mathrm{S}*}(t)$ and $\theta_\mathrm{S}(t)$ that can be separately profiled over the course of the surface reaction.

The kinetic model described above has been applied to the quantitative analysis of time-resolved SPRI and SPFS measurements of the catalytic behavior of RNase H on surface-immobilized RNA–DNA heteroduplexes. Figure 8.5 shows the $\Delta\%R$ loss observed in real-time SPRI measurements due to the selective removal of RNA from the surface at enzyme concentrations ranging from 0.5 to 4 nM. The analysis of the SPRI kinetic curves (shown as solid lines in Figure 8.5) using eqs. (8.8)–(8.10) yielded best-fit values of $3.4 \times 10^6\,\mathrm{M}^{-1}\cdot\mathrm{s}^{-1}$, $0.1\,\mathrm{s}^{-1}$, $1.0\,\mathrm{s}^{-1}$ and 180 for k_a, k_d, k_cat and β, respectively. Also, the analysis showed $\theta_\mathrm{ES}(t)$ remained very small ($\sim 10^{-3}$) throughout the

reaction with $k_{cat} \gg k_a[E]$. This means that once adsorbed, RNase H reacts very quickly and is immediately released from the surface. The observed k_{cat} value of $1.0\,s^{-1}$ is significantly faster than k_{cat} measured in a similar study 65 for the surface hydrolysis of double-stranded DNA by Exonuclease III ($k_{cat} = 0.01\,s^{-1}$). In this surface reaction, the time-dependent SPRI signal initially increased before an eventual overall decrease due to the loss of the complementary strand in the surface DNA duplex. This behavior is qualitatively very different from that of the RNase H reaction in Figure 8.5, where at no point was a net increase in SPRI signal observed.

Since enzyme adsorption and surface duplex hydrolysis both contribute to the measured SPRI response, some assumptions on the relative contributions of both reaction steps are required when using our kinetic model. Therefore, to characterize the surface enzyme reaction completely it is important to obtain an independent set of *in situ* surface kinetic measurements. In the case of RNase H, this was achieved using fluorescently labeled RNA and applying the technique of SPFS [64]. The loss in SPFS signal due to enzymatic hydrolysis of the surface attached RNA is a direct measure of $\theta_S(t)$ and was analyzed in a similar manner to the SPRI data for various enzyme concentrations. The k_a, kd and k_{cat} best-fit values obtained from the SPFS measurements were almost identical with the values obtained from the SPRI data described above, indicating that fluorescence labeling of RNA does not significantly affect k_{cat}.

8.3.2 RNase H Amplified Detection of DNA

The first major breakthrough in the application of surface enzyme processes to greatly improve the sensitivity of SPRI bioaffinity measurements was the use of the RNase H surface process for the amplified detection of DNA [48,49]. Figure 8.6a shows how this enzymatic amplification methodology works. An RNA probe microarray is exposed to a solution containing both target DNA and RNase H. When a target DNA molecule binds to a complementary RNA probe array element, RNase H recognizes the formed RNA–DNA heteroduplex and selectively hydrolyzes the RNA strand (Step 1). The target DNA is released back into solution and is free to bind to another surface RNA probe and RNase H will again hydrolyze the RNA in the surface heteroduplex (Step 2). This repeated target binding–enzymatic hydrolysis–target release will continue until all the RNA probe molecules are removed from the surface (Step 3). Amplification is achieved because only a very small number of target DNA molecules are required to produce a large change in SPRI signal.

The sensitivity of RNase H amplified SPRI was found to be sufficient for the detection of DNA at concentrations as low as 1 fM. Consequently, we have been able to directly detect target sequences in a human genomic DNA sample *without* PCR amplification. Figure 8.6b shows an SPRI difference image of a three-component RNA microarray following a 4 h exposure to a genomic DNA sample. At the R1 and R2 elements, which contain sequences designed to bind specifically to the TSPY gene on the Y chromosome, a decrease in SPRI

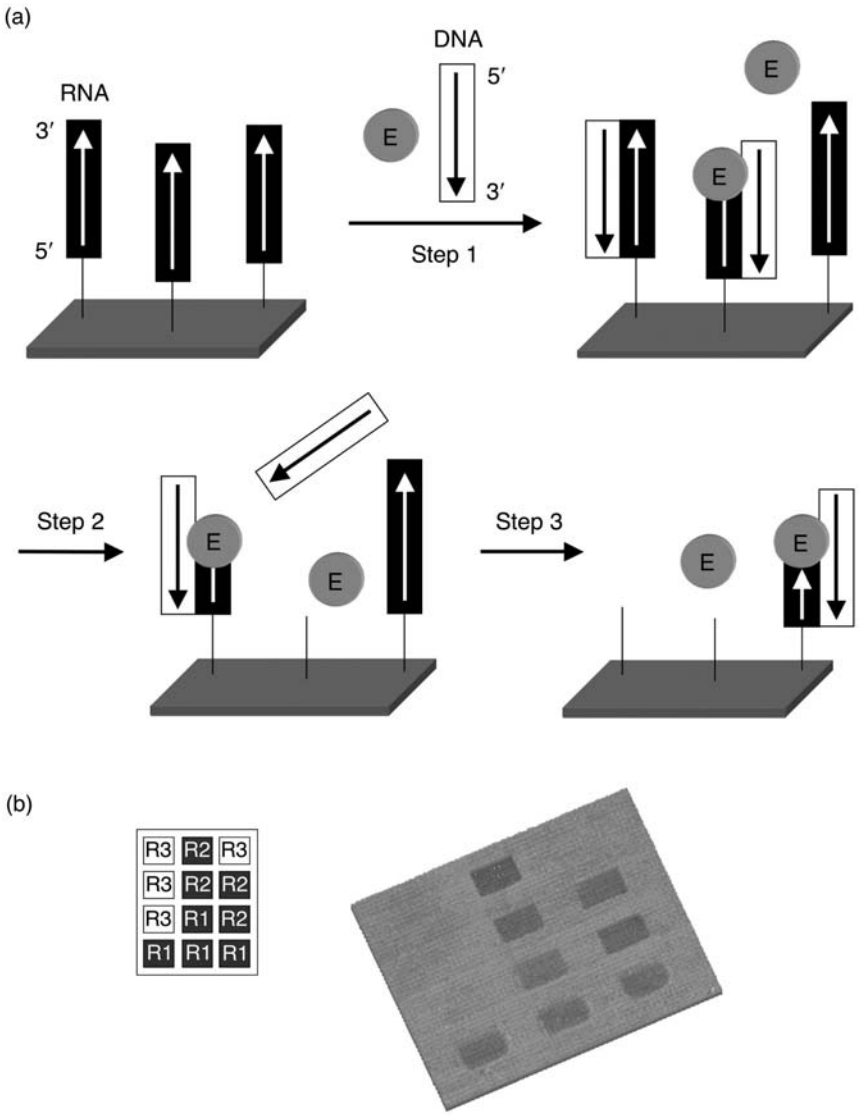

Figure 8.6 (a) Schematic outlining enzymatically amplified SPRI methodology using an RNA microarray for the detection of target DNA. (b) An SPRI difference image obtained for the detection of male genomic DNA in the presence of RNase H. A schematic of the three-component RNA microarray is also shown where R1 and R2 are specifically designed to bind to the TSPY gene on the Y chromosome and R3 is a negative control sequence. Reprinted with permission from reference 48.

signal (–0.7%) was observed[2], whereas no change in SPRI signal was observed at either the R3 elements or the array background. The concentration of the TSPY gene sequences in commercially available male genomic DNA was estimated to be 7 fM [48]. In addition to human genomic DNA, this enzymatically amplified SPRI method can be applied to the ultrasensitive detection and identification of DNA and RNA from viruses and bacteria.

8.3.3 Fabrication of RNA Microarrays with RNA-DNA Surface Ligation Chemistry

A second example of how surface enzyme processes can be applied to enhance the biosensing capabilities of SPRI is the use of ligation chemistry to create RNA microarrays from DNA microarrays. The ability to fabricate stable and active single stranded RNA (ssRNA) microarrays is essential for a successful RNase H amplified SPRI measurement and will also promote the use of RNA microarrays for the study of RNA–protein, RNA–RNA and other bioaffinity interactions. Despite the many potential benefits of RNA microarrays, at present only a handful of reports are available on the fabrication of RNA microarrays in the literature [48,49,66–70]. The use of modified RNA sequences such as biotinylated RNA [66,69,70] or thiol-modified RNA [48,49] can be time consuming and costly with also the increased possibility of RNA degradation during both the modification and surface attachment procedures. To address these problems, we have recently developed two novel RNA fabrication strategies utilizing two different enzymes: (i) T4 DNA ligase and (ii) T4 RNA ligase [47,71]. Both of these enzymes catalyze the ligation of unmodified RNA onto a DNA microarray, but only T4 DNA ligase requires the use of a complementary DNA template sequence [47].

Figure 8.7 outlines a simplified schematic for the creation of an ssRNA microarray using T4 DNA ligase. A single-stranded (ssDNA) microarray is first prepared by chemically attaching 3′-thiol modified, 5′-phosphorylated ssDNA. These anchor DNA array elements (D_A) are then exposed to a solution containing T4 DNA ligase and both probe RNA (R_P) and template ssDNA (D_T), which will hybridize to the D_A surface. Following the formation of a phosphodiester bond between the 5′-phosphate of D_A and the 3′-hydroxyl group of R_P the array surface is thoroughly rinsed with 8 M urea in order to denature and remove the DNA template and any T4 DNA ligase, resulting in the creation of biologically active ssRNA array elements. The SPRI difference image [b – a] in Figure 8.7 shows a $\Delta\%R$ increase of $2.2 \pm 0.3\%$ following the ligation of 24mer RNA [47]. We also found that the original ssDNA microarray could be regenerated with RNase H hydrolysis allowing the surface ligation process to be repeated to create a new RNA microarray. This is because RNase H specifically cleaves the phosphodiester bonds in the RNA component of the DNA-RNA heteroduplex (formed by D_C hybridization–adsorption on R_P) to

[2] Note that the minimum change in SPRI reflectivity that can be measured is around 0.08%.

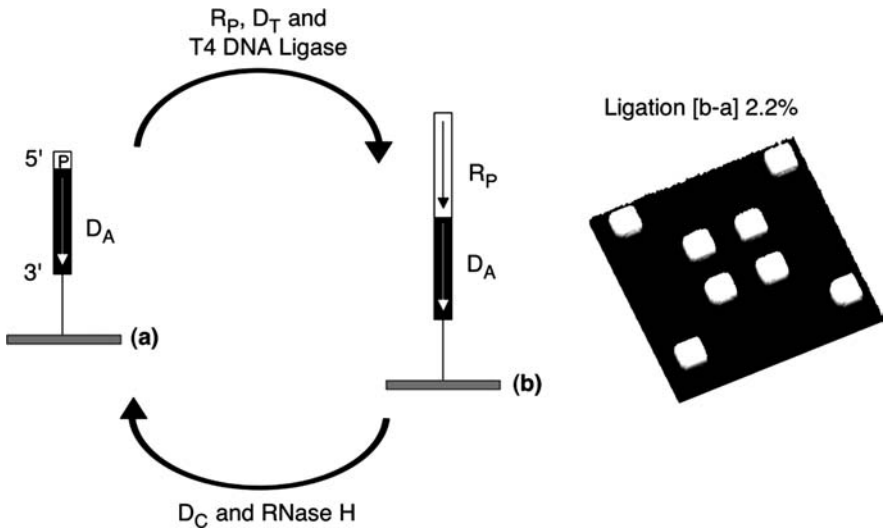

Figure 8.7 Simplified schematic of the fabrication of a renewable ssRNA microarray via RNA–DNA ligation chemistry followed by RNase H hydrolysis. The ssRNA microarray was created by the selective ligation of RNA (R_P) to D_A elements of a two-component DNA microarray in the presence of a DNA template (D_T). Hybridization of complementary DNA (D_C) on to the ligated ssRNA followed by the selective hydrolysis of R_P using RNase H regenerates the original 5′-phosphorylated ssDNA surface. The right inset shows a representative *in situ* SPRI difference image [b – a] obtained by subtracting images acquired before and after RNA ligation. Reprinted with permission from reference 47.

produce 5′-phosphate and 3′-OH termini. This ligation-hydrolysis cycle could be repeated up to three times using the same ssDNA microarray without any degradation in SPRI signal. In addition, when the ligated microarray was used for the detection of 1 pM DNA *via* RNase H amplification, the initial rate of change in $\Delta\%R$ observed was over 20 times faster than that observed with microarrays prepared using thiol modified RNA. This is attributed to an increase in RNase H activity due to the anchor DNA sequence spacing R_P further from the gold surface.

A second example of the application of surface ligation chemistry for the fabrication of ssRNA microarrays is the use of the enzyme T4 RNA ligase, which does not require a complementary DNA template sequence [71]. To create a multi-component RNA microarray using this approach, solutions containing both enzyme and RNA probe were delivered onto individual array DNA elements *via* spotting. Following completion of the ligation reaction, the microarray was rinsed with 8 M urea to remove any enzyme and non-ligated ssRNA from the surface. As outlined in Figure 8.8a, the prepared bioactive ssRNA array elements can then be directly applied for the study of RNA–

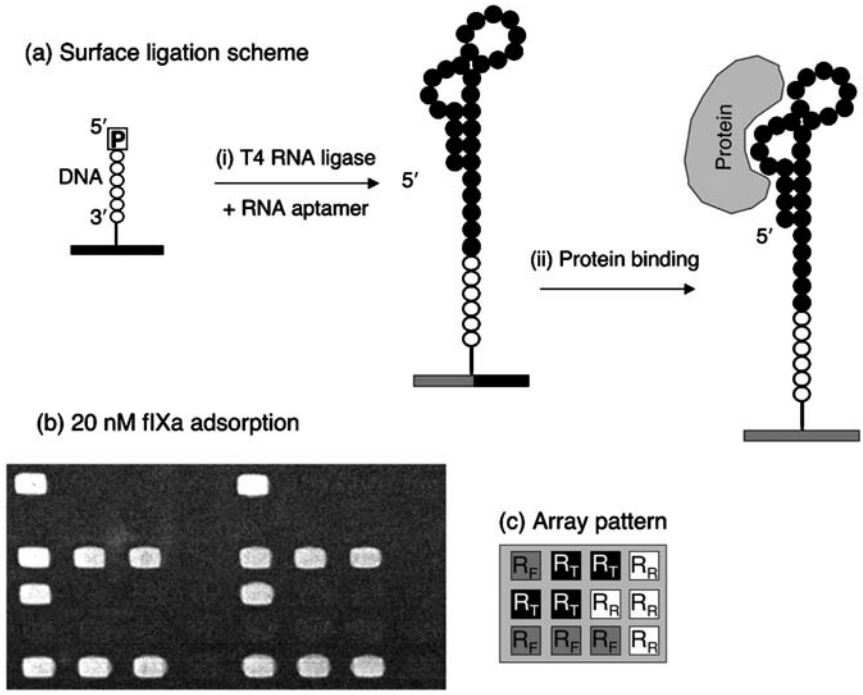

Figure 8.8 (a) Schematic showing the creation of an RNA aptamer microarray via RNA–DNA surface ligation chemistry using T4 RNA ligase. DNA and RNA bases are shown as open circles and filled circles, respectively. Step (i): microarray elements composed of 5′-phosphorylated ssDNA are individually exposed to solutions containing ssRNA aptamer molecules and T4 RNA ligase. This results in the formation of a phosphodiester bond between the 3′-hydroxyl of the ssRNA and the 5′-phosphate of the ssDNA. Step (ii): after ligation, the surface is rinsed with 8 M urea to remove the enzyme and non-ligated ssRNA. The ssRNA aptamer microarray is then used for the study of protein–aptamer binding events. (b) SPRI difference image obtained for the specific adsorption of 20 nM fIXa on the R_F array elements of a three-component microarray. (c) A pattern of a three-component aptamer array where R_F has a high binding affinity towards fIXa and R_T and R_R are negative control aptamer sequences.

protein bioaffinity interactions. Figure 8.8b shows an SPRI difference image obtained for the adsorption of 20 nM human factor IXa (fIXa) on a three-component RNA aptamer microarray. The array pattern is shown in Figure 8.8c, where R_F has a strong binding affinity for fIXa with both R_C and R_R aptamer variants acting as negative controls. In addition to the screening of different aptamer sequences, these ligated RNA microarrays can also be applied to the ultrasensitive detection of protein biomarkers [71].

8.4 Nanoparticle-amplified SPRI Biosensing

A second method for increasing the sensitivity of SPRI bioaffinity measurements by several orders of magnitude is the use of functionalized gold nanoparticles, an approach which is also completely compatible with the use of surface enzyme chemistry. Nanoparticle amplified SPRI detection of DNA was originally demonstrated by He *et al*. who used DNA-modified nanoparticles to achieve a detection limit of 10 pM in a sandwich assay format [30]. Although the dependence of the SPR response as a function of both nanoparticle size and the nanoparticle–planar film separation distance has been investigated by several groups [72–74], nanoparticles are not yet routinely applied for enhanced SPRI bioaffinity sensing. In this section, two novel methodologies combining surface enzyme reactions and nanoparticle-enhanced SPRI measurements are described for (i) the analysis of single nucleotide polymorphisms (SNPs) in genomic DNA and (ii) the femtomolar detection of microRNAs (miRNAs[3]) in a total RNA sample. In both studies, DNA-modified gold nanoparticles ($\sim$13 nm diameter) were utilized with a maximum absorbance at 525 nm. The surface plasmon excitation wavelength in our SPRI measurements is 830 nm. Therefore, the amplification in SPRI signal is primarily due to changes in refractive index and not absorptive coupling between the gold nanoparticles and thin gold film. A theoretical description of nanoparticle SPR can be found in Chapter 2.

8.4.1 Single Nucleotide Polymorphism Genotyping

The development of new methods for the rapid, multiplexed detection and identification of single nucleotide polymorphisms (SNPs) in human genomic DNA samples is attracting major interest as these methods can be used to accelerate the discovery of specific disease-related mutations and also for large-scale human genetic variation studies. In principle, SPRI measurement with DNA microarrays is an ideal candidate technique for SNP genotyping. Various researchers have employed both conventional SPRI and single-channel SPR formats to detect single base mismatches in DNA by hybridization adsorption [24,77–80]. However, the SPRI detection limit of 1 nM described in Section 8.2 is insufficient for SNP genotyping of *unamplified* genomic DNA samples where the detection of single base pairs in a DNA sequence at a concentration of 1 pM or better is required.

In order to demonstrate that SPRI can be used for multiplexed SNP genotyping, we developed a novel approach that involves the sequence-specific ligation of target DNA to an ssDNA microarray followed by the nanoparticle-amplified SPRI detection of the surface ligated product. As outlined in Figure 8.9, a solution containing the 36mer target T, a 5′-phosphorylated ssDNA ligation probe L and the enzyme *Taq* DNA ligase (E) is introduced to a two-

[3] MicroRNAs are a new class of small, non-coding RNA molecules (19–23mers) that can regulate gene expression in both plants and animals [76,76].

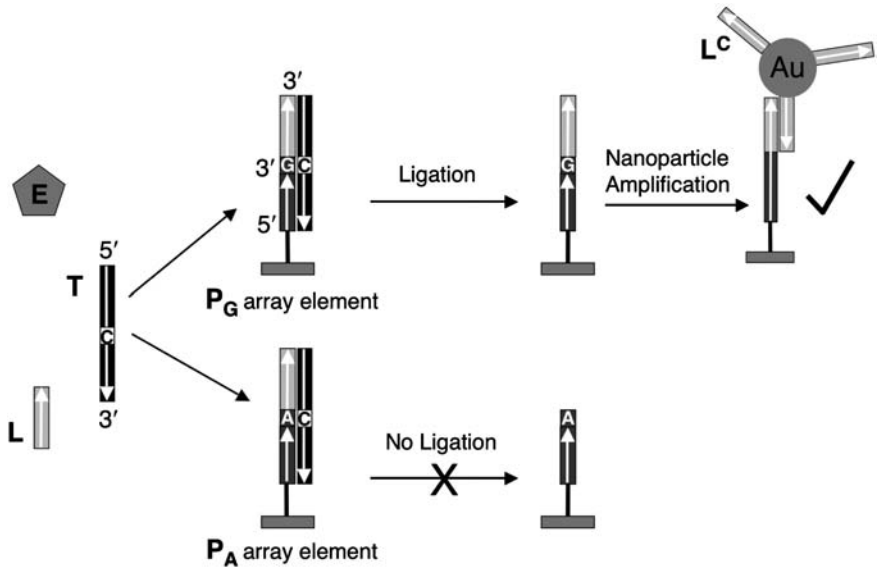

Figure 8.9 Schematic of SNP genotyping method based on the combined use of surface ligation chemistry and nanoparticle enhanced SPRI. Reprinted with permission from reference 44.

component ssDNA microarray containing the probes P_G and P_A [44]. The two array probe DNA sequences differ only by the last nucleotide at their 3′-termini (G for P_G and A for P_A). The target DNA molecules hybridize simultaneously to the ligation probes and the array probes, resulting in the formation of two different surface complexes, L–T–P_G and L–T–P_A. Single base pair selectivity is achieved because *Taq* DNA ligase will only catalyze the formation of a phosphodiester bond between the juxtaposed P and L probes when they are both perfectly complementary to the hybridized target. Here, the ligation probe will be specifically ligated to P_G but not to P_A. Following an 8 M urea wash to remove any target, non-ligated probe and enzyme from the microarray, SPRI detection of the ligated L–P_G array elements is achieved through the hybridization adsorption of gold nanoparticles modified with ssDNA 16mers (L^C) which are complementary to the ligation probe sequence.

Prior to performing experiments using real genomic DNA samples, the sensitivity and single base specificity of this advanced SPRI methodology was established using synthetic target oligonucleotides. A four-component array was designed consisting of three 20mer probe sequences P_A, P_C and P_G that are identical except for the last nucleotide at their 3′-termini (A, C and G, respectively) and also a poly T sequence P_N, which serves as a negative control. Specific ligation of the 16mer L probe to only one of the array components could be detected for 36mer T concentrations as low as 1 Pm [44].

Having established the detection limit of this SNP genotyping method, we then applied the same microarray design to screen the PCR products of human genomic DNA samples for a possible point mutation in the *BRCA1* gene that is associated with breast cancer. In this case, probe P_G is the perfect complement to the wild-type allele, probe P_C is the perfect complement to the mutant allele in NA13710, while probe P_A is the perfect complement to the mutant allele in NA14637. Both mutant samples were obtained from the Coriell Institute [44]. The SNP genotyping results for the wild-type and NA14637 samples are shown in Figures 8.10a and b, respectively. The SPRI difference image in Figure 8.10a shows an increase in reflectivity only at the P_G array elements, indicating that the genotype of the wild-type DNA sample is a C–C homozygote. However, in Figure 8.10(b), a Δ%R increase was observed at both the P_G and P_A array elements, identifying the NA14637 sample as a C–T heterozygote. The NA13710 sample (data not shown) was identified as a C–G heterozygote.

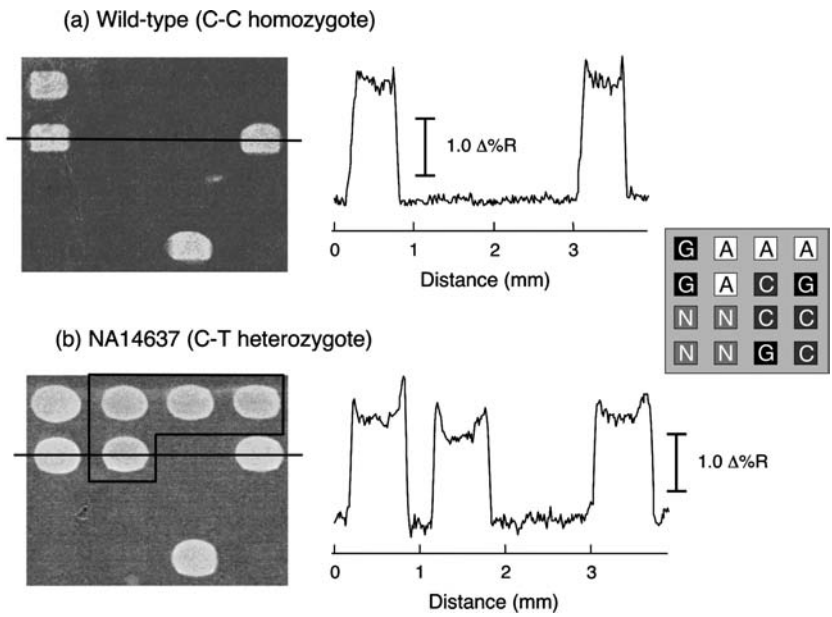

Figure 8.10 SNP genotyping of 1 nM PCR amplicons of genomic DNA samples (a) wild-type and (b) NA14637. Both SPRI difference images measure the hybridization adsorption of L^C-modified nanoparticles on a four-component DNA microarray (P_A, P_C, P_G and P_N) after the surface ligation and denaturation steps are completed. The SPRI difference image (left) and corresponding line profiles (middle) are shown next to the array pattern (right). An increase in SPRI signal was observed only at the P_G array elements for the (a) wild-type sample identifying it as being a C–C homozygote. For the (b) NA14637 mutant sample, an SPRI signal increase was observed at both the P_G and P_A (boxed) elements identifying it as a C–T heterozygote. Reprinted with permission from reference 44.

These experiments successfully demonstrate for the first time that SPRI can be applied for multiplexed SNP genotyping achieving both high specificity and sensitivity. The detection limit of 1 pM is comparable to that typically reported for fluorescence imaging measurements of DNA microarrays [81,82] and we expect that this detection limit will further improve with the incorporation of enzymatic amplification methods.

8.4.2 MicroRNA Detection

A final example of an advanced SPRI biosensing methodology is the use of both a surface poly(A) polymerase reaction and nanoparticle amplification for the ultrasensitive microarray detection of microRNAs (miRNAs) down to a concentration of 10 fM. In the previous example, improved sensitivity was obtained from nanoparticle adsorption only. However, in this case, both the enzyme reaction and DNA-coated nanoparticles contribute to the amplification of the SPRI response. As indicated in the left inset in Figure 8.11, poly(A) polymerase selectively catalyzes the multiple addition of adenosine residues to the 3′-OH end of ssRNA molecules resulting in the formation of long poly(A)

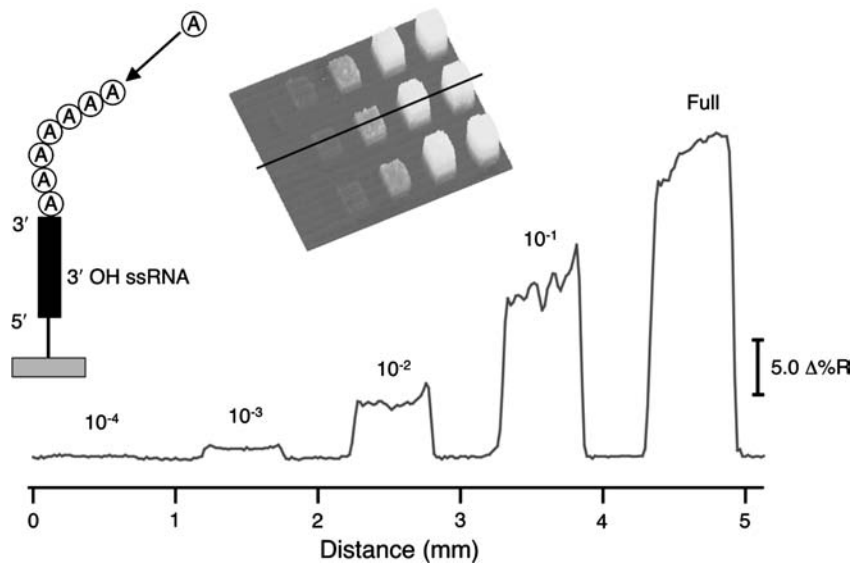

Figure 8.11 SPRI difference image (top middle) and corresponding line profile (bottom) obtained after a surface polyadenylation reaction (left inset) on a microarray composed of array elements with relative ssRNA surface coverages ranging from 10^{-1} to 10^{-4}. The array elements were created by diluting a 1 mM solution of thiol-modified ssRNA (R_1) with 1 mM thiol-modified ssDNA solution prior to surface immobilization and surface polyadenylation reaction at the 3′-end of the surface-attached ssRNA substrate.

tails. To characterize the surface polymerase reaction, 5′-thiol-modified, 3′-OH ssRNA was covalently attached to the gold surface via a surface thiol–maleimide reaction [34,49] to create an ssRNA monolayer with free 3′-hydroxyl groups that are accessible to the enzyme. Figure 8.11 shows an SPRI difference image along with the corresponding line profile following the completion of the polyadenylation reaction on a microarray where the fractional surface coverage of ssRNA ranged from a full monolayer to 10^{-4}. The diluted array elements were prepared by mixing a 1 mM solution of thiol-modified ssRNA with a 1 mM solution of a non-interacting thiol-modified ssDNA sequence of similar length in a ratio that varied from 1:10 to $1:10^4$. An hour was sufficient for completion of the polyadenylation reaction with the data in Figure 8.11, clearly showing that SPRI reflectivity changes could be detected at ssRNA surface coverages of around 10^{-3}.

A further gain in SPRI sensitivity can be achieved by the hybridization adsorption of T_{30} DNA-coated nanoparticles on the surface polyadenylated ssRNA. Figure 8.12 compares the total change in SPRI reflectivity measured after both polyadenylation and nanoparticle adsorption with the SPRI signal obtained after the polyadenylation step only [34]. When a 10 nM nanoparticle

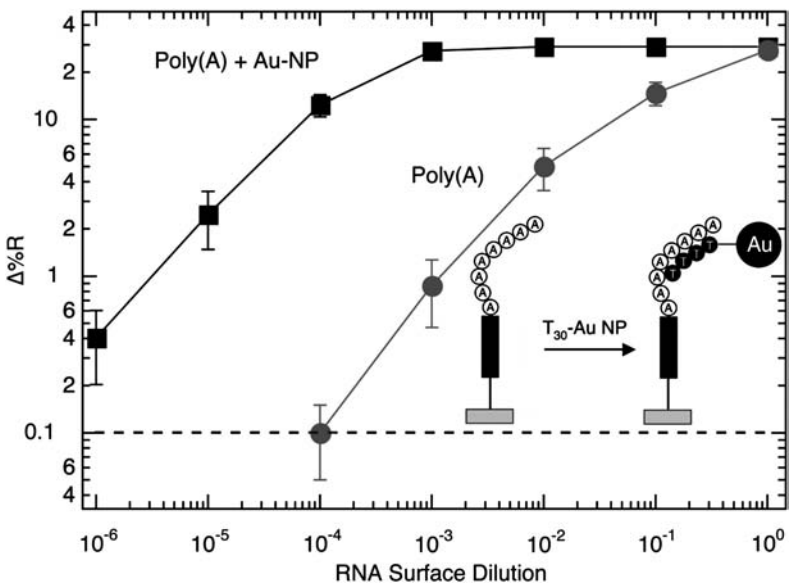

Figure 8.12 SPR reflectivity changes as a function of ssRNA surface coverage after surface polyadenylation reaction (●) and after nanoparticle (NP) adsorption on a surface where the polyadenylation reaction has already occurred (■). The inset shows the scheme of the hybridization–adsorption of T_{30}-coated gold nanoparticles (Au-NP) on the poly(A) tail formed at the 3′-end of the surface-attached ssRNA molecules. The dashed line indicates the minimum detectable SPRI response signal. Reprinted with permission from reference 34.

solution was employed, the SPRI signal responded linearly at ssRNA fractional surface coverages ranging from 10^{-6} to 10^{-4}. At higher coverages, the SPRI responsivity decreases with signal saturation observed at a ΔR of $\sim$25%, as expected from theory [53]. The remarkably low value of 10^{-6} corresponds to an ssRNA surface density of 5×10^6 molecules cm^{-2}or just $\sim$10 000 RNA molecules on a 500 μm square array element! These measurements can be used to estimate what concentration of target miRNA in solution would be required to achieve a similar surface coverage following hybridization adsorption onto a complementary nucleic acid microarray. At low miRNA concentrations (C), the fractional surface coverage (θ) can be described using the equation $\theta = K_{ads}C$. Given a Langmuir adsorption coefficient (K_{ads}) of $10^8\,M^{-1}$, a θ of 10^{-6} corresponds to an miRNA concentration of 10 fM.

Figure 8.13 shows how this polyadenylation–nanoparticle amplification scheme can be applied to the ultrasensitive detection of miRNAs using SPRI [34]. The recent surge in interest in miRNAs has led to an increased need for new methods that can perform multiplexed, quantitative analyses at very low target concentrations [83–85]. The first step (i) in our miRNA detection methodology involves the sequence-specific hybridization adsorption of the miRNA target on a single-stranded locked nucleic acid (LNA) microarray.

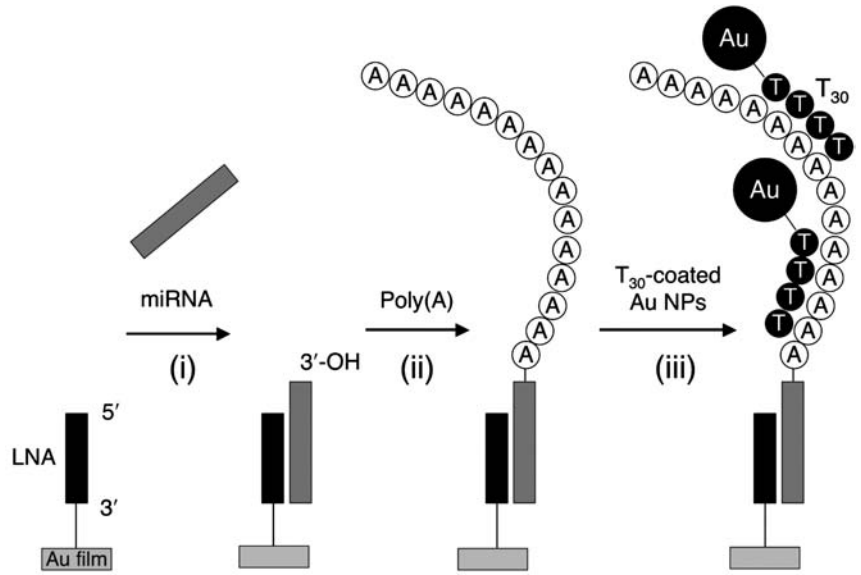

Figure 8.13 Detection of microRNAs using a combination of surface polyadenylation chemistry and nanoparticle-amplified SPRI. Step (i): hybridization adsorption of miRNA onto a complementary LNA array element. Step (ii): poly(A) tail addition at the 3′-end of surface bound miRNAs using poly(A) polymerase. Step (iii): hybridization–adsorption of T_{30}-coated Au nanoparticles to poly(A) tails. Reprinted with permission from reference 34.

LNAs are nucleic acid analogues containing one or more nucleotides modified with an extra bridge connecting the 2′-O and 4′-C atoms of the ribose moiety; the RNA–LNA binding strength ($\sim 10^8\,M^{-1}$) is at least 10 times greater than that associated with RNA–DNA heteroduplex formation [83]. The presence of the surface-bound miRNA is then detected with SPRI following polyadenylation (step ii) and T_{30}-coated nanoparticle adsorption (step iii). Initial measurements were performed using synthetic analogues of the target miRNA molecules with the SPRI response was found to increase linearly over a concentration range of 10–500 fM. Both the detection limit and linear response range could be adjusted by varying the nanoparticle concentration. At miRNA concentrations of 100 pM and above, polyadenylation was sufficient to detect the presence of miRNA without nanoparticle amplification.

As a final demonstration, the surface polyadenylation-nanoparticle amplification methodology was applied to the multiplexed detection of three different miRNAs present in a total RNA sample extracted from mouse liver tissue. A four-component microarray was constructed containing three LNA probes designed to bind to the known miRNA sequences [34,84], miR-16, miR-122b and miR-23b, with a DNA probe used as a negative control. A 250 ng RNA sample in a volume of 500 µl was circulated over the microarray surface repeatedly for 4 h followed by surface amplification. Analysis of the resulting SPRI difference image (Figure 8.14a) and corresponding line profile (Figure 8.14c) clearly shows the miR-122b sequence as the most abundant with a measured ΔR of 9.7% [34]. Having already calibrated the linear SPRI response range using synthetic analogues of the target sequences we were able to estimate miRNA concentrations of 20 fM, 50 fM and 2 pM for miR-16, miR-23b and miR-122b, respectively. Further verification of the concentration of the least abundant miRNA (miR-16) was obtained by repeating the measurement with the addition of 100 fM synthetic miR-16. As shown in Figures 8.14b and c, a 5-fold increase in SPRI signal was observed only at the miR-16 probe array elements. These experiments demonstrate unequivocally that polyadenylation–nanoparticle amplified SPRI measurements can be used to profile miRNA sequences quantitatively in biological samples. The current detection limit of 5 amol (10 fM in 500 µl) opens up the possibility of complete miRNA profiling with SPRI using very small amounts of sample (<250 ng).

8.5 Summary and Outlook

This chapter highlights some of the recent advances that we have made in improving the microarray-based biosensing capabilities of SPRI. The continual development of new surface attachment chemistries and array fabrication methods on gold film surfaces has resulted in a large variety of biomolecular interactions that have been studied in a multiplexed format using SPRI. Furthermore, the selectivity, sensitivity and applicability of SPRI bioaffinity measurements can be greatly enhanced by incorporating surface enzyme reactions into the detection scheme. The ability to detect unlabeled DNA sequences

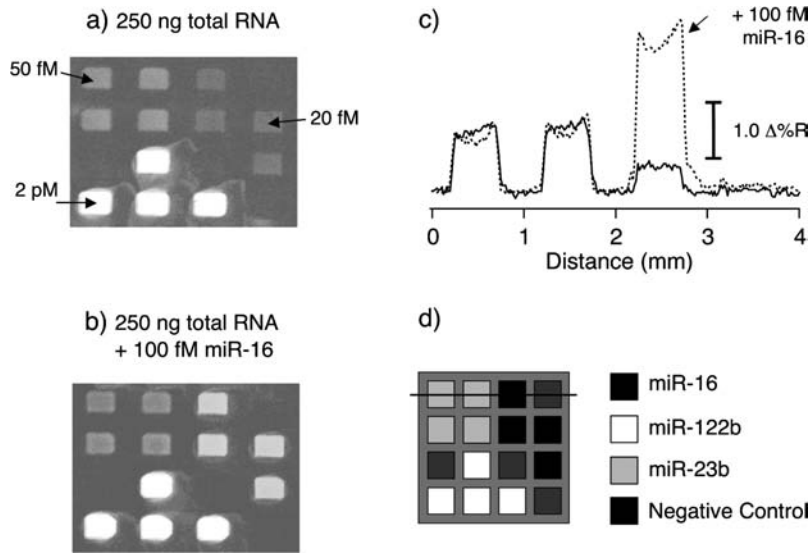

Figure 8.14 Quantitative analysis of miRNAs from 250 ng of mouse liver total RNA using polyadenylation–nanoparticle amplified SPRI measurements. (a) SPRI difference image obtained by subtracting images acquired before and after the nanoparticle amplification step. (b) An SPRI difference image obtained from a separate chip using the same total RNA concentration as the top image plus the addition of 100 fM synthetic miR-16. (c) Comparison of line profiles taken from both SPRI difference images with the solid and dashed lines corresponding to top and bottom images respectively. (d) Schematic of the four-component LNA probe microarray and the line profile location. Reprinted with permission from reference 34.

at concentrations as low as 1 fM using RNase H amplified SPRI is a remarkable improvement compared with the previous nanomolar detection limit of SPRI based on hybridization absorption only. Also, we found the combined use of surface enzyme reactions and nanoparticle-enhanced SPRI to be particularly powerful. This allowed us to demonstrate for the first time that SPRI can be applied for SNP genotyping; the surface *Taq* DNA ligase reaction enhanced the specificity of the SNP detection while DNA-coated nanoparticles amplified the SPRI response. Even greater improvements in sensitivity were achieved through the combined use of a surface poly(A) polymerase reaction and DNA-coated nanoparticles, which we used to simultaneously detect multiple miRNAs present at concentrations ranging from 20 fM to 2 pM in a total RNA sample.

The level of sensitivity obtained using these combined enzyme–nanoparticle amplified SPRI methods is equal to or better than that of fluorescence imaging measurements of DNA microarrays, where a detection limit of 1 pM is typically reported [79,80]. Another strength of SPRI *versus* fluorescence is the ability to

monitor directly multi-affinity interactions involving the adsorption of two or more species on a single surface probe, which is important for the development of more complex multi-step assays. Furthermore, the nucleic acid enzymes described in this chapter are only some of the many possible enzymes (*e.g.* proteases, kinases) that can be utilized on biomolecules attached to microarray surfaces. In the case of more complex surface enzymatic processes, the combined use of SPFS and SPRI measurements will support the development of more complicated surface kinetic models and also help optimize the surface enzyme reaction through changes in surface density and vertical spacing of the immobilized substrate. The surface enzyme reactions at gold surfaces described in this chapter can also be coupled with fluorescence or electroactive labeled molecules; this opens up the possibility of creating new enzymatic methods which combine SPRI with other surface-sensitive detection techniques. We expect that, as more advanced surface amplification methods are developed for ultrasensitive microarray bioaffinity measurements, the technique of SPRI will continue to grow in importance as an invaluable research tool that can be applied to many areas of modern biotechnology research.

8.6 Questions

1. A significant improvement in SPR imaging instrumentation was achieved by using a non-coherent light source instead of coherent laser excitation. (A) Suggest some reasons why and (B) outline other features of the optical setup required for SPRI measurements.
2. Most surface bioaffinity measurements utilize the specific adsorption of target biomolecules (T) from solution onto a surface that has been chemically modified with probe biomolecules (P). If the target and probe interact in a simple 1:1 ratio, then in the absence of bulk transport the surface reaction can be represented in the form

$$\mathrm{T} + \mathrm{P} \underset{k_\mathrm{d}}{\overset{k_\mathrm{a}}{\rightleftharpoons}} \mathrm{TP}$$

   where TP is the surface bound target–probe complex. Both P and TP are surface species, and in the Langmuir approximation their surface concentrations Γ_P and Γ_TP are linked to the total concentration of surface sites G_tot by

$$\Gamma_\mathrm{tot} = \Gamma_\mathrm{P} + \Gamma_\mathrm{TP}$$

   A. If we define θ as the fraction of occupied surface sites, $\theta = \Gamma_\mathrm{TP}/\Gamma_\mathrm{tot}$, write down the differential equation for the time evolution of θ (*i.e.* $\mathrm{d}\theta/\mathrm{d}t = \cdots$) using k_a, k_d and the bulk concentration $[T]$.
   B. Find the steady-state equilibrium surface coverage θ_eq, which is obtained in the steady-state approximation ($\mathrm{d}\theta/\mathrm{d}t = 0$). This equation

defines the Langmuir adsorption coefficient $K_{ads} = k_a/k_d$. What is θ_{eq} at a bulk concentration equal to $1/K_{ads}$?

3. One of the main factors that determine the SPRI detection limit for DNA hybridization adsorption is how low a fractional surface coverage of target DNA on the gold chip surface can actually be measured. At low target concentrations the solution to question 2B can be approximated as $\theta_{eq} = K_{ads}[T]$. In the text, the DNA detection limit reported for long-range SPRI measurements was 1 nM, with a value of 1 pM described for nanoparticle-enhanced SPRI detection. In the case of RNase H amplified SPRI, a detection limit of 1 fM was reported. For the detection limits of 1 nM, 1 pM and 1 fM, calculate θ_{eq}, Γ_{TP} and estimate the number of target DNA molecules contributing to a change in signal within an array element that has an area of $500 \times 500\,\mu m$. Assume $K_{ads} = 2 \times 10^7\,M^{-1}$ and a surface density of DNA probe molecules of 5×10^{12} molecules cm^{-2} with all probes available for target binding.
4. In the text, several examples where surface enzyme reactions form the basis of advanced SPRI biosensing measurements were demonstrated. Equations (8.8)–(8.11) describe the reaction of an enzyme in solution with a surface-immobilized substrate that couples Langmuir adsorption/desorption kinetics with the rate of the surface enzyme reaction. The time-dependent SPRI signal $\Delta\%R(t)$ responds to both enzyme adsorption and the loss of DNA or RNA substrate from the gold surface (see Figure 8.5, inset) and can be represented by $\Delta\%R(t) = \theta_{ES}$–$\theta_{S*}$.
   A. Using simple Euler integration methods (which can be easily applied in Excel, Igor Pro or any mathematics software) with the initial conditions $\theta_s = 1$ and $\theta_{ES} = \theta_{S*} = 0$ at time $t = 0$, try to simulate the surface kinetic reaction described in eqs. (8.8)–(8.11). Generate two sets of plots showing θ_{ES}, θ_{S*},θ_S and $\Delta\%R(t)$ *versus* time using the following parameter values:
      Parameter Set 1 where $k_{cat} > k_a$[E]:
      $k_a = 1 \times 10^6\,M^{-1} \cdot s^{-1}$
      $k_d = 0.025\,s^{-1}$
      $k_{cat} = 2.5\,s^{-1}$
      $[E] = 2.5 \times 10^{-7}\,M$
      $\beta = 0$.
      Parameter Set 2 where $k_{cat} < k_a$ [E]:
      $k_a = 1 \times 10^6\,M^{-1} \cdot s^{-1}$
      $k_d = 0.025\,s^{-1}$
      $k_{cat} = 0.025\,s^{-1}$
      $[E] = 2.5 \times 10^{-7}\,M$
      $\beta = 0$.
   B. To demonstrate the impact of mass transport effects on the kinetics of the surface enzyme reaction, replot Parameter Set 2 using $\beta = 50$.

5. As well as in this chapter and Chapter 2, gold nanoparticles are used for sensitive detection of biomolecular interactions. What is the fundamental difference in applying these particles in SPR instruments?
6. In Section 8.3.1, the enzymatic amplification technique is described and applies the principle of slow surface kinetics with respect to fast kinetics in a homogeneous solution. One of the prerequisites of the enzymatic reaction is that the product of the enzymatic reaction is a precipitate. Another way of improving sensitivity is the detection of an enzyme-catalyzed desorption process. Describe this method.
7. A detection limit of 5 amol (10 fM in 500 µl) of miRNA with SPRI is shown for very small amounts of sample (<250 ng). Which two tricks were applied to achieve this limit of detection?

8.7 Acknowledgements

This research was funded by the National Institutes of Health (2RO1 GM059622-04) and the National Science Foundation (CHE-0551935). The authors would like to thank Dr. S. Fang for obtaining the SPRI difference image shown in Figure 8.11.

Uncited References

75,76

References

1. D.J. Lockhart and E.A. Winzeler, *Nature*, 2000, **405**, 827.
2. P.O. Brown and D. Botstein, *Nat. Genet.*, 1999, **21**, 33.
3. R.B. Stoughton, *Annu. Rev. Biochem.*, 2005, **74**, 53.
4. J.M. Thomson, J. Parker, C.M. Perou and S.M. Hammond, *Nat. Methods*, 2004, **1**, 47.
5. R.L. Stears, T. Martinsky and M. Schena, *Nat. Med.*, 2003, **9**, 140.
6. Y.P. Bao, M. Martin Huber, T. Wei, S.S. Marla, J.J. Storhoff and U.R. Müller, *Nucleic Acids Res.*, 2005, **33**, e15.
7. D. Gerion, F. Chen, B. Kannan, A. Fu, W.J. Parak, D.J. Chen, A. Majumdar and A.P. Alivisatos, *Anal. Chem.*, 2003, **75**, 4766.
8. P.F. Predki, *Curr. Opin. Chem. Biol.*, 2004, **8**, 8.
9. H. Zhu and M. Snyder, *Curr. Opin. Chem. Biol.*, 2003, **7**, 55.
10. G. Macbeath and S.L. Schreiber, *Science*, 2000, **289**, 1760.
11. S.F. Kingsmore, *Nat. Rev. Drug Discov.*, 2006, in press.
12. P. Bertone and M. Snyder, *FEBS J.*, 2005, **272**, 5400.
13. M. Srivastava, O. Eidelman, C. Jozwik, C. Paweletz, W. Huang, P.L. Zeitlin and H.B. Pollard, *Mol. Genet. Metab.*, 2006, **87**, 303.

AQ1

14. W. Gao, R. Kuick, R.P. Orchekowski, D.E. Misek, J. Qiu, A.K. Greenberg, W.N. Rom, D.E. Brenner, G.S.S. Omenn, B.B. Haab and S.M. Hanash, *BMC Cancer*, 2005, **5**, 110.
15. W. Hickel, D. Kamp and W. Knoll, *Nature*, 1989, **339**, 186.
16. B. Rothenhäusler and W. Knoll, *Nature*, 1988, **332**, 615.
17. E. Yeatman and E.A. Ash, *Electron. Lett.*, 1987, **23**, 1091.
18. H.J. Lee, A.W. Wark and R.M. Corn, *Langmuir*, 2006, **22**, 5241.
19. K.S. Phillips, T. Wilkop, J.-J. Wu, R.O. Al-Kaysi and Q. Cheng, *J. Am. Chem. Soc.*, 2006, **128**, 9590.
20. L.K. Wolf, D.E. Fullenkamp and R.M. Georgiadis, *J. Am. Chem. Soc.*, 2005, **127**, 17453.
21. T. Wilkop, Z. Wang and Q. Cheng, *Langmuir*, 2004, **20**, 11141.
22. M. Kyo, K. Usui-Aoki and H. Koga, *Anal. Chem.*, 2005, **77**, 7115.
23. V. Kanda, P. Kitov, D.R. Bundle and M.T. McDermott, *Anal. Chem.*, 2005, **77**, 7497.
24. A. Okumura, Y. Sato, M. Kyo and H. Kawaguchi, *Anal. Biochem.*, 2005, **339**, 328.
25. M. Kyo, T. Yamamoto, H. Motohashi, T. Kamiya, T. Kuroita, T. Tanaka, J.D. Engel, B. Kawakami and M. Yamamoto, *Genes Cells*, 2004, **9**, 153.
26. J.S. Shumaker-Parry and C.T. Campbell, *Anal. Chem.*, 2004, **76**, 907.
27. J.S. Shumaker-Parry, M.H. Zareie, R. Aebersold and C.T. Campbell, *Anal. Chem.*, 2004, **76**, 918.
28. V. Kanda, J.K. Kariuki, D.J. Harrison and M.T. McDermott, *Anal. Chem.*, 2004, **76**, 7257.
29. E.A. Smith and M.R. Corn, *Appl. Spectrosc.*, 2003, **57**, 320A.
30. L. He, M.D. Musick, S.R. Nicewarner, F.G. Salinas, S.J. Benkovic, M.J. Natan and C.D. Keating, *J. Am. Chem. Soc.*, 2000, **122**, 9071.
31. L.A. Lyon, W.D. Holliway and M.J. Natan, *Rev. Sci. Instrum.*, 1999, **70**, 2076.
32. S.F. Gonzalez, M.J. Krug, M.E. Nielsen, Y. Santos and D.R. Call, *J. Clin. Microbiol.*, 2004, **42**, 1414.
33. S. Sengupta, K. Onodera, A. Lai and U. Melcher, *J. Clin. Microbiol.*, 2003, **41**, 4542.
34. S. Fang, H.J. Lee, A.W. Wark and R.M. Corn, *J. Am. Chem. Soc.*, 2006, **128**, 14044.
35. C.E. Jordan, A.G. Frutos, A.J. Thiel and R.M. Corn, *Anal. Chem.*, 1997, **69**, 4939.
36. A.J. Thiel, A.G. Frutos, C.E. Jordan, R.M. Corn and L.M. Smith, *Anal. Chem.*, 1997, **69**, 4948.
37. B.P. Nelson, A.G. Frutos, J.M. Brockman and R.M. Corn, *Anal. Chem.*, 1999, **71**, 3928.
38. B. Frey and R.M. Corn, *Anal. Chem.*, 1996, **68**, 3187.
39. J.M. Brockman, A.G. Frutos and R.M. Corn, *J. Am. Chem. Soc.*, 1999, **121**, 8044.
40. A.G. Frutos, J.M. Brockman and R.M. Corn, *Langmuir*, 2000, **16**, 2192.

41. E. Smith, M.J. Wanat, Y. Cheng, S.V.P. Barreira, A.G. Frutos and R.M. Corn, *Langmuir*, 2001, **17**, 2502.
42. H.J. Lee, T.T. Goodrich and R.M. Corn, *Anal. Chem.*, 2001, **73**, 5525.
43. H.J. Lee, D. Nedelkov and R.M. Corn, *Anal. Chem.*, 2006, **78**, 6504.
44. Y. Li, A.W. Wark, H.J. Lee and R.M. Corn, *Anal. Chem.*, 2006, **78**, 3158.
45. A.W. Wark, H.J. Lee and R.M. Corn, *Anal. Chem.*, 2005, **77**, 3904.
46. H.J. Lee, Y. Li, A.W. Wark and R.M. Corn, *Anal. Chem.*, 2005, **77**, 5096.
47. H.J. Lee, A.W. Wark, Y. Li and R.M. Corn, *Anal. Chem.*, 2005, **77**, 7832.
48. T.T. Goodrich, H.J. Lee and R.M. Corn, *J. Am. Chem. Soc.*, 2004, **126**, 4086.
49. T.T. Goodrich, H.J. Lee and R.M. Corn, *Anal. Chem.*, 2004, **76**, 6173.
50. E.A. Smith, M.G. Erickson, A.T. Ulijasz, B. Weisblum and R.M. Corn, *Langmuir*, 2003, **19**, 1486.
51. G.J. Wegner, H.J. Lee and R.M. Corn, *Anal. Chem.*, 2002, **74**, 5161.
52. G.J. Wegner, A.W. Wark, H.J. Lee, E. Codner, T. Saeki, S. Fang and R.M. Corn, *Anal. Chem.*, 2004, **76**, 5677.
53. B.P. Nelson, T.E. Grimsrud, M.R. Liles, R.M. Goodman and R.M. Corn, *Anal. Chem.*, 2001, **73**, 1.
54. D.J. O'Shannessy, M. Brigham-Burke, K.K. Soneson, P. Hensley and I. Brooks, *Anal. Biochem.*, 1993, **212**, 457.
55. G.G. Neminger, P. Tobiska, J. Homola and S.S. Yee, *Sens. Actuators B*, 2001, **74**, 145.
56. F. Yang, G.W. Bradberry and J.R. Sambles, *Phys. Rev. Lett.*, 1991, **66**, 2030.
57. J.C. Quail, J.G. Rako and H.J. Simon, *Opt. Lett.*, 1983, **8**, 377.
58. D. Sarid, *Phys. Rev. Lett.*, 1981, **47**, 1927.
59. W.N. Hansen, *J. Opt. Soc. Am.*, 1968, **58**, 380.
60. http://www.corninfo.ps.uci.edu/calculations.html.
61. A. Kasry and W. Knoll, *Appl. Phys. Lett.*, 2006, **89**, 101106.
62. C. Bourdillon, C. Demaille, J. Moiroux and J. Saveant, *J. Am. Chem. Soc.*, 1999, **121**, 2401.
63. P. Schuck and A.P. Minton, *Anal. Biochem.*, 1996, **240**, 262.
64. S. Fang, H.J. Lee, A.W. Wark, H.M. Kim and R.M. Corn, *Anal. Chem.*, 2005, **77**, 6528.
65. H.J. Lee, A.W. Wark, T.T. Goodrich, S. Fang and R.M. Corn, *Langmuir*, 2005, **21**, 4050.
66. E.J. Cho, J.R. Collet, A.E. Szafranska and A.D. Ellington, *Anal. Chim. Acta*, 2006, **564**, 82.
67. J.R. Collett, E.J. Cho, J.F. Lee, M. Levy, A.J. Hood, C. Wan and A.D. Ellington, *Anal. Biochem.*, 2005, **338**, 113.
68. T. Mori, A. Oguro, T. Ohtsu and Y. Nakamura, *Nucleic Acids Res.*, 2004, **32**, 6120.
69. T.G. McCauley, N. Hamaguchi and M. Stanton, *Anal. Biochem.*, 2003, **319**, 244.
70. M.B. Murphy, S.T. Fuller, P.M. Richardson and S.A. Doyle, *Nucleic Acids Res.*, 2003, **31**, e110.

AQ1 71. Y. Li, H.J. Lee, R.M. Corn, *Nucleic Acids Res*., 2006, **34**, in press.
72. L. He, E.A. Smith, M.J. Natan and C.D. Keating, *J. Phys. Chem. B*, 2004, **108**, 10973.
73. L.A. Lyon, D.J. Pena and M.J. Natan, *J. Phys. Chem. B*, 1999, **103**, 5826.
74. L.A. Lyon, M.D. Musick and M.J. Natan, *Anal. Chem*., 1998, **70**, 5177.
75. R.W. Carthew, *Curr. Opin. Genet. Dev*., 2006, **16**, 203.
76. D. Bartel, *Cell*, 2004, **116**, 281.
77. T. Endo, K. Kerman, N. Nagatani, Y. Takamura and E. Tamiya, *Anal. Chem*., 2005, **77**, 6976.
78. J. Liu, S. Tian, L. Tiefenauer, P.E. Nielsen and W. Knoll, *Anal. Chem*., 2005, **77**, 2756.
79. A.W. Peterson, L.K. Wolf and R.M. Georgiadis, *J. Am. Chem. Soc*., 2002, **124**, 14601.
80. K. Nakatani, S. Sando and I. Saito, *Nat. Biotechnol*., 2001, **19**, 51.
81. H.-P. Lehr, M. Reimann, A. Brandenburg, G. Sulz and H. Klapproth, *Anal. Chem*., 2003, **75**, 2414.
82. T. Livache, E. Maillart, N. Lassalle, P. Mailley, B. Corso, P. Guedon, A. Roget and Y. Levy, *J. Pharm. Biomed. Anal*., 2003, **32**, 687.
83. M. Castoldi, S. Schmidt, V. Benes, M. Noerholm, A.E. Kulozik, M.W. Hentze and M.U. Muckenthaler, *RNA*, 2006, **12**, 913.
84. T. Babak, W. Zhang, Q. Morris, B.J. Blencowe and T.R. Hughes, *RNA*, 2004, **10**, 1813.
85. P.T. Nelson, D.A. Baldwin, L.M. Scearce, J.C. Oberholtzer, J.W. Tobias and Z. Mourelatos, *Nat. Methods*, 2004, **1**, 155.
86. B.P. Nelson, M.R. Liles, K. Frederick, R.M. Goodman and R.M. Corn, *Environ. Microbiol*., 2002, **4**, 735.
87. J.M. Brockman, B.P. Nelson and R.M. Corn, *Annu. Rev. Phys. Chem*., 2000, **51**, 41.
88. E.A. Smith, W.D. Thomas, L.L. Kiessling and R.M. Corn, *J. Am. Chem. Soc*., 2003, **125**, 6140.
89. G.J. Wegner, H.J. Lee, G. Marriott and R.M. Corn, *Anal. Chem*., 2003, **75**, 4740.

Chapter 8: Author Queries

Note: Please check all the equation because there is a problem with uncommon font conversion.

1. Update?
2. Update?
3. Some of the symbols were corrupted: please insert.